Eur. Phys. J. Plus (2021) 136:960
https://doi.org/10.1140/epjp/s13360-021-01923-w

THE EUROPEAN PHYSICAL JOURNAL PLUS

Regular Article

Numerical study of MHD natural heat transfer of non-Newtonian, carbon nanotube-water nanofluid inside an internally finned annulus

Hooman Hadidi[1], **Seyed Mahmood Mousavi**[1], **Mehdi Ghalambaz**[2,3,a]

[1] School of Mechanical Engineering, Shiraz University, 71936-16548 Shiraz, Iran
[2] Institute of Research and Development, Duy Tan University, Da Nang 550000, Vietnam
[3] Faculty of Electrical – Electronic Engineering, Duy Tan University, Da Nang 550000, Vietnam

Received: 26 May 2021 / Accepted: 31 August 2021
© The Author(s), under exclusive licence to Società Italiana di Fisica and Springer-Verlag GmbH Germany, part of Springer Nature 2021

Abstract In this paper, a numerical analysis of natural convection of a non-Newtonian nanofluid flow in a finned annulus employing a finite element approach is presented. The computational domain is affected by an external magnetic field. This study is carried out for various parameters, including Hartmann number, Rayleigh number, nanoparticles volume fraction, power-law index, Prandtl number, and fin length ratio. Results show that as the Hartmann number increases, the magnetic force opposes the buoyancy force and generally suppresses the convection process. Also, it is shown that the effect of Hartmann number alteration on the equivalent thermal conductivity (K_{eq}) weakens for smaller *Ra* numbers. Besides, the influence of the Hartmann number on decreasing the net convective heat transfer drop as the power-law index increases, and augmentation of the power-law index causes K_{eq} to decline. The results reveal that by adding nanoparticles to the base fluid, the enhancement in total heat transfer is more intensified in low Rayleigh numbers with a reduction in the difference between K_{eq} values for various volume fractions as the Hartmann number rises. Furthermore, the effect of the Hartmann number on decreasing the net convective heat transfer increases for lower power-law index values, i.e., variations of the Hartmann number has a stronger influence on K_{eq} for power-law fluids with $n < 1$ in comparison with those with $n > 1$.

1 Introduction

Natural convection inside concentric cylinders is encountered in various thermal engineering applications, including food processing, solar collectors, drying technologies, cooling electronic devices, heat exchangers, solar power collectors, and glass production. Adding nanoparticles to the fluid has proved as an efficient way to enhance heat transfer [1–4]. In

[a] e-mail: mehdighalambaz@duytan.edu.vn (corresponding author)

the past years, researchers have used different kinds of nanoparticles for this purpose [5–8]. Furthermore, magnetohydrodynamic (MHD) is an important way to control heat transfer in various engineering fields. Sheikholeslami et al. [9] employed lattice Boltzmann method (LBM) to explore magnetohydrodynamic (MHD) flow using water-based nanofluid with copper nanoparticles inside two concentric cylinders. Numerical results for flow and heat transfer characteristics are reported for different Hartmann number values, nanoparticle volume fraction, Rayleigh number ($Ra = 10^4$,10^5 and 10^6), and aspect ratio. They observed an increase in the enhancement ratio due to the Hartmann number augmentation and Rayleigh number decrease. In another numerical study [10], simulation of natural heat transfer in a cavity confining nanofluid was carried out. In their study, various obstacles were utilized. Their results revealed that the obstacles diminish the heat transfer remarkably, and this effect is much better observable at higher values of the Rayleigh number. Similar conclusions were made by Malekpour et al. [11] in their investigation corresponding to natural convection of nanofluids in an I shape compartment under the effect of a magnetic field.

Second law analyses have also been carried out utilizing various measures to compute the entropy generation. Kefayati [12] employed LBM to examine natural convection heat transfer of the laminar flow corresponding to the non-Newtonian nanofluids within a square-shaped cavity under the effect of a magnetic field. They showed that as the volume fraction and Rayleigh number increase, heat transfer, entropy generation, and friction within the enclosure increase as well.

Selimefendigil and Chamkha [13] performed a numerical investigation on mixed convection of CuO-water nanofluid in a three-dimensional cavity under the effect of an external magnetic field. It was revealed that the recirculation zone is suppressed by the magnetic field leading to the overall heat transfer improvement.

Alsabery et al. [14] studied MHD mixed convection of nanofluids in a lid-driven cavity heated by a triangular wall using the finite element method. It was observed that as a result of the Hartmann augmentation, thermophoresis and Brownian motion increase, which cause the nanoparticles migrate more easily within the enclosure.

Tayebi and Chamkhah [15] carried out a numerical study of entropy generation and natural convection of Cu -Al2O3/water hybrid nanofluid within a square enclosure in the presence of a wavy circular conductive cylinder under the effect of a magnetic field. It was shown that increasing buoyancy forces leads to the entropy generation augmentation and decreasing Bejan number.

Karimipour et al. [16] explored the heat transfer of nanofluid flow in a long microchannel in the presence of an external magnetic field using the finite volume method. Their results revealed that a higher slip coefficient is associated with a smaller *Nu* number and larger slip velocity, particularly at larger Hartmann numbers. Alizadeh et al. [17] examined the thermodynamics of mixed convection of a nanofluid in a stagnation flow configuration in the presence of an external magnetic field. In keeping with others, they showed that increases in Hartmann number improve the thermodynamic irreversibility.

In another numerical study [18], the heat transfer within a cavity composed of nanofluid was investigated. It was shown that when the Grashof number rises, the temperature gradient increases, as well. The effects of Lorentz forces on nanofluid flow patterns were simulated by Kandelousi [19]. It was shown that as the Kelvin forces get strong, the natural convection inside the enclosure weakens. In another research [20], the effect of asymmetric heating on the Nusselt number enhancement through a microchannel was explored. It was shown that Lorentz forces could improve the heat transfer by approximately 42%. The effects of radiation heat transfer on the concentration of nanoparticles have been investigated by Hayat et al. [21]. It was revealed that variations of the temperature inside the channel decrease with

the rise of thermal radiation. The effect of the magnetic field's direction on the flow style was studied by Malvandi [22]. It was shown that the anisotropic characteristic of thermal conductivity can be altered by Lorentz forces. Most recently, Saeed et al. [23] examined the impacts of magnetic forces upon the flow characteristic of a non-Newtonian fluid inside a microchannel. Among other results, these authors showed that the extent of the magnetic effect on the heat transfer and thermodynamics of the system depends heavily upon the wall thickness of the microchannel.

Natural heat transfer of a nanofluid in a tilted wavy enclosure was examined in ref. [24]. Their outputs illustrated that changing the angle of inclination leads to convective heat transfer augmentation. Sheikholeslami and Ganji [25] considered Marangoni convection to explore CuO-H_2O nanofluid convective heat transfer in the presence of magnetic field utilizing similarity solution. Their results indicated that the rate of heat transfer is an augmenting function of CuO volume fraction. CuO-H_2O nanofluid convection heat transfer in a lid-driven porous cavity was studied under the effect of the magnetic field by Sheikholeslami [26]. He investigated the shape influence of nanoparticles and the Brownian motion effect on the properties of nanofluids. The outputs showed that the heat transfer is enhanced due to the increase in Darcy and Reynolds number, while it diminishes with increases in Lorentz forces. Sheikholeslami and Shamlooei [27] investigated Fe_3O_4-H_2O nanofluid hydrothermal features under the effect of an external magnetic field and thermal radiation. Results revealed that at higher buoyancy forces, thermal radiation leads to a more remarkable effect on the convection heat transfer.

It can be understood from the preceding review of literature that although there are numerous works considering MHD free heat transfer of nanofluids, so far, there has been no study of an annulus containing non-Newtonian nanofluid in the presence of an external magnetic field, to the best of our knowledge. Given the practical importance of these enclosures, the current lack of thermal analysis reflects an important shortcoming. To address this, in this paper, natural convection of a non-Newtonian nanofluid under the effect of a magnetic field inside a finned annulus is simulated by a finite element approach. The effects of numerous parameters, including Hartmann number, volume fraction, power-law index, fin length, Rayleigh number, and Prandtl number, are examined.

2 Problem definition

The computational domain investigated in this work is illustrated in Fig. 1a. It is composed of an infinitely long horizontal annulus confining non-Newtonian carbon nanotube (CNT)-water nanofluid in the presence of a vertical magnetic field with the intensity of B_o. Table 1 contains the thermophysical properties of nanoparticles and base fluid. The inner cylinder has a higher temperature (T_i) than the outer cylinder (T_o). The fins have the same temperature as that of the inner cylinder (T_i), and their temperature has been kept constant during the simulations. In this study, the fluid flow is considered to be incompressible, steady, 2D, and laminar. Constant physical properties have been assumed for the fluid, except the body force, where the Boussinesq approximation is employed for the variations of the density. Furthermore, due to the axisymmetric nature of the flow configuration, a two-dimensional analysis is conducted.

2.1 Governing equations

According to the assumptions mentioned previously, the governing equations are given as follows [31]:

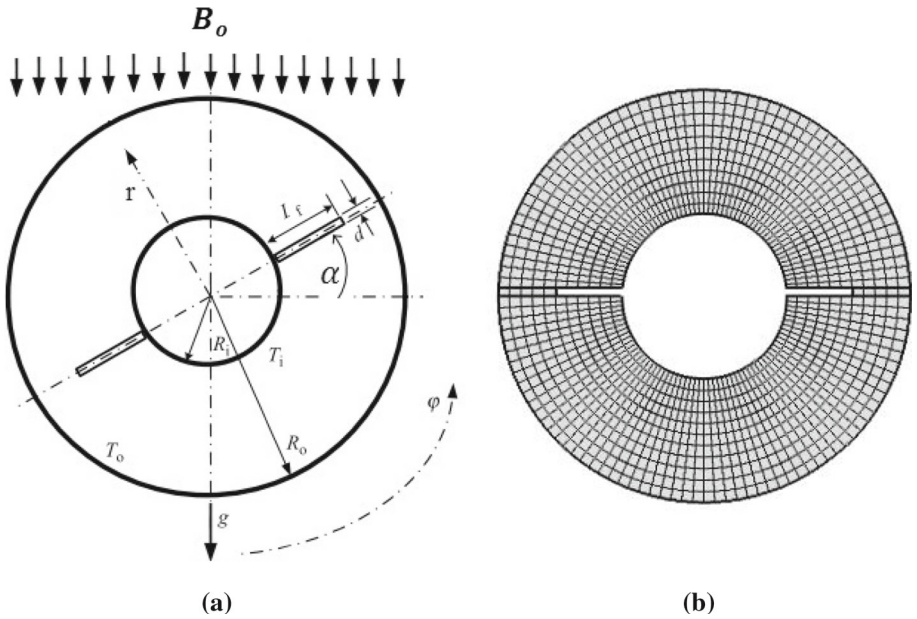

Fig. 1 **a** Schematic view of the annulus with two internal fins. **b** The structured mesh of the computational domain

Table 1 Thermophysical and electrical properties of CNT nanoparticles and base fluid

	Cp (J/kg K)	K (W/m K)	ρ (kg/m^3)	σ (S/m)
Water	4179	3000	997.2	30,000
CNT	765 [30]	0.612 [29]	3970	5.5×10^{-6} [28]

Continuity of mass:

$$\nabla . \overrightarrow{V} = 0 \tag{1}$$

Momentum equation:

$$\nabla . \left(\rho_{nf} \overrightarrow{V} \overrightarrow{V} \right) = -\nabla (p) + \nabla . \overline{\overline{\tau}} + (\rho \beta)_{nf} \overrightarrow{g} (T - T_c) + \overrightarrow{f}_k \tag{2}$$

Energy equation:

$$\nabla . \left(\overrightarrow{V} T \right) = \nabla . (\lambda_{nf} \nabla T) \tag{3}$$

in which, $\overrightarrow{V}$, p, T, ρ and $\overrightarrow{g}$ represent velocity, pressure, temperature, density, and gravitational acceleration, respectively. $\overline{\overline{\tau}}$ indicates the stress tensor. The last term in Eq. (2) indicates the magnetic body force, which for the vertical uniform magnetic force in this study, it has only one nonzero component as $\sigma_{nf} B_0^2 \overrightarrow{u}$ [16, 32], in which $\overrightarrow{u}$ represents the velocity components in the x-direction. Considering the direction of the body force, it is convenient to write the governing equations in a 2D Cartesian coordinate system. Consequently, the governing equations of continuity, momentum, and energy will have the following forms [12, 16, 32]:

$$\frac{\partial u}{\partial x} + \frac{\partial v}{\partial y} = 0 \tag{4}$$

$$u\frac{\partial u}{\partial x}+v\frac{\partial u}{\partial y}=\frac{1}{\rho_{nf}}\left[-\frac{\partial p}{\partial x}+\left(\frac{\partial \tau_{xx}}{\partial x}+\frac{\partial \tau_{xy}}{\partial y}\right)-\sigma_{nf}B_0^2u\right] \tag{5}$$

$$u\frac{\partial v}{\partial x}+v\frac{\partial v}{\partial y}=\frac{1}{\rho_{nf}}\left[-\frac{\partial p}{\partial y}+\left(\frac{\partial \tau_{xy}}{\partial x}+\frac{\partial \tau_{yy}}{\partial y}\right)+\left(\rho\beta\right)_{nf}g(T-T_c)\right)\right] \tag{6}$$

$$u\frac{\partial T}{\partial x}+v\frac{\partial T}{\partial y}=\gamma_{nf}\left(\frac{\partial^2 T}{\partial x^2}+\frac{\partial^2 T}{\partial y^2}\right) \tag{7}$$

where u and v represent the velocity components along x and y directions.

Moreover, λ_{nf} indicate the nanofluid's thermal diffusivity and can be given by:

$$\lambda_{nf}=\frac{K_{nf}}{(\rho C_p)_{nf}} \tag{8}$$

in which, K_{nf} represents the nanofluid's thermal conductivity. The density,ρ_{nf}, the heat capacity, $(\rho C_p)_{nf}$, and the thermal expansion coefficient corresponding to the nanofluid $(\rho\beta)_{nf}$ are computed by [16]:

$$\rho_{nf}=(1-\omega)\rho_f+\omega\rho_s \tag{9}$$

$$\left(\rho C_p\right)_{nf}=(1-\omega)\left(\rho C_p\right)_f+\omega\left(\rho C_p\right)_s \tag{10}$$

$$(\rho\beta)_{nf}=(1-\omega)(\rho\beta)_f+\omega(\rho\beta)_s \tag{11}$$

where ω represents the volume fraction of the nanoparticles. Subscripts *f, s,* and *nf* indicate base fluid, solid, and nanofluid, respectively.

The shear stress tensor ($\overline{\overline{\tau}}$) in a non-Newtonian nanofluid that obeys the power-law model can be obtained by:

$$\overline{\overline{\tau}}=\mu_{nf}\overline{\overline{\dot{\gamma}}} \tag{12}$$

where $\overline{\overline{\dot{\gamma}}}$ and μ_{nf} can be written as follows, respectively [33, 34]:

$$\overline{\overline{\dot{\gamma}}}=\nabla\overrightarrow{V}+(\nabla\overrightarrow{V})^t \tag{13}$$

$$\mu_{nf}=\frac{\mu_f}{(1-\omega)^{2.5}} \tag{14}$$

$$\mu_f=m||\dot{\gamma}||^{(n-1)};\ ||\dot{\gamma}||=\sqrt{\frac{\overline{\overline{\dot{\gamma}}}:\overline{\overline{\dot{\gamma}}}}{2}} \tag{15}$$

in which $(\nabla\overrightarrow{V})^t$ indicates the transpose of $\nabla\overrightarrow{V}$. Moreover, n and m represent power-law index consistency coefficients, respectively, and μ_f as the base fluid's viscosity is given by [12]:

$$\mu_f=m\left\{2\left[\left(\frac{\partial u}{\partial x}\right)^2+\left(\frac{\partial v}{\partial y}\right)^2\right]+\left(\frac{\partial v}{\partial x}+\frac{\partial u}{\partial y}\right)^2\right\}^{\frac{(n-1)}{2}} \tag{16}$$

In a 2D Cartesian coordinate system, the shear stress tensor is obtained by [12]:

$$\tau_{ij}=2\mu_{nf}D_{ij}=\frac{\mu_f}{(1-\omega)^{2.5}}\left(\frac{\partial u_i}{\partial x_j}+\frac{\partial u_j}{\partial x_i}\right) \tag{17}$$

where D_{ij} represents the strain-rate tensor for the 2D Cartesian coordinate.

The boundary conditions are as follows [35, 36]:

- For the inner cylinder (hot wall):

$$u = v = 0 \quad T = T_i$$

- For the outer cylinder (cold wall):

$$u = v = 0 \quad T = T_o \tag{18}$$

Besides, the thermal conductivity (K_{nf}) and the electrical conductivity (σ_{nf}) associated with the nanofluid can be obtained by the following equations, respectively [16]:

$$\frac{K_{nf}}{K_f} = \frac{K_s + 2K_f + 2\omega\left(K_f - K_s\right)}{K_s + 2K_f - 2\omega\left(K_f - K_s\right)} \tag{19}$$

$$\frac{\sigma_{nf}}{\sigma_f} = 1 + \frac{3(\eta - 1)\omega}{(\eta + 2) - (\eta - 1)\omega} \tag{20}$$

where $\eta = \frac{\sigma_s}{\sigma_f}$.

2.2 Non-dimensional form of governing equations

To obtain the non-dimensionalized form Eqns. (4)-(7), the following non-dimensional variables have been introduced:

$$\begin{aligned} x^* &= \frac{x}{L} y^* = \frac{y}{L} u^* = \frac{u}{\left(\frac{\lambda_f}{L}\right) Ra^{0.5}}, v^* = \frac{v}{\left(\frac{\lambda_f}{L}\right) Ra^{0.5}} \\ p^* &= \frac{p}{\rho_{nf}\left(\frac{\lambda_f}{L}\right)^2 Ra}, \theta = \frac{T - T_0}{T_i - T_0}, \chi_1^* = \frac{(x - R_i)}{(R_o - R_i)} \end{aligned} \tag{21}$$

By using these dimensionless parameters, Eqns. (4)-(7) are converted to the following dimensionless forms:

$$\frac{\partial u^*}{\partial x^*} + \frac{\partial v^*}{\partial y^*} = 0 \tag{22}$$

$$\begin{aligned} u^* \frac{\partial u^*}{\partial x^*} + v^* \frac{\partial v^*}{\partial y^*} = &- \frac{\partial p^*}{\partial x^*} + \frac{\Pr}{\sqrt{Ra}} \frac{\rho_f}{\rho_{nf}} \frac{1}{(1-\omega)^{2.5}} \\ &\times \left[2 \frac{\partial}{\partial x^*} \left(\frac{\mu_f}{m} \frac{\partial u^*}{\partial x^*} \right) + \frac{\partial}{\partial y^*} \left(\frac{\mu_f}{m} \left(\frac{\partial u^*}{\partial y^*} + \frac{\partial v^*}{\partial x^*} \right) \right) \right] \\ &- \frac{\rho_f}{\rho_{nf}} \frac{1}{(1-\omega)^{2.5}} \frac{\sigma_{nf}}{\sigma_f} \frac{\Pr Ha^2}{\sqrt{Ra}} u^* \end{aligned} \tag{23}$$

$$\begin{aligned} u^* \frac{\partial u^*}{\partial x^*} + v^* \frac{\partial v^*}{\partial y^*} = &- \frac{\partial p^*}{\partial y^*} + \frac{\Pr}{\sqrt{Ra}} \frac{\rho_f}{\rho_{nf}} \frac{1}{(1-\omega)^{2.5}} \\ &\times \left[2 \frac{\partial}{\partial y^*} \left(\frac{\mu_f}{m} \frac{\partial v^*}{\partial y^*} \right) + \frac{\partial}{\partial x^*} \left(\frac{\mu_f}{m} \left(\frac{\partial u^*}{\partial y^*} + \frac{\partial v^*}{\partial x^*} \right) \right) \right] + \Pr \frac{(\rho\beta)_{nf}}{\rho_{nf}\beta_f} \theta \end{aligned} \tag{24}$$

$$u^* \frac{\partial \theta}{\partial x^*} + v^* \frac{\partial \theta}{\partial y^*} = \frac{1}{\sqrt{Ra}} \frac{\gamma_{nf}}{\gamma_f} \left(\frac{\partial^2 \theta}{\partial x^{*2}} + \frac{\partial^2 \theta}{\partial y^{*2}} \right) \tag{25}$$

The Prandtl and Rayleigh numbers have the following forms, respectively [37]:

$$\mathrm{Pr} = \frac{\mu_f}{\rho_f \gamma} \tag{26}$$

$$Ra = \frac{\rho_f g \beta_f \Delta T L^3}{\mu_f \gamma} \tag{27}$$

where L is the characteristics length ($L = \mathrm{R_o}\text{-}\mathrm{R_i}$), and ΔT is defined as: $\Delta T = T_i - T_o$.

Hartmann number is defined as [16]:

$$Ha = B_0 L \left(\frac{\sigma_f}{\mu_f} \right)^{0.5} \tag{28}$$

The average equivalent thermal conductivity (K_{eq}) is defined as [38]:

$$K_{eq} = \frac{Nu}{Nu_{cond}} \tag{29}$$

where

$$Nu = [(Nu_{cond})^{15} + (Nu_{conv})^{15}]^{1/15} \tag{30}$$

$$Nu_{conv} = \left[\frac{1}{Nu_i} + \frac{1}{Nu_o} \right]^{-1} \tag{31}$$

$$Nu_{cond} = \frac{2}{\ln(\frac{R_o}{R_i})} \tag{32}$$

in which, R represents the radius of the cylinder, and subscripts i and o indicate the inner and outer cylinder, respectively.

3 Numerical procedure

To discretize the governing equations, a finite element scheme (FEM) on a structure grid has been employed. Approximation of the convective fluxes has been carried out with the second-order upwind scheme. The convergence criteria for solving Eqs. (1) – (3) have been chosen as 10^{-6}. Details on the grids used for the computations and validation tests are given in the following sections.

3.1 Grid independence study

As illustrated in Fig. 1b, structural grids with 20 elements on each of the concentric cylinders are used. To ensure our numerical study's accuracy, a grid independence investigation was performed. Figure 2 depicts dimensionless temperature θ for various mesh number for φ=90°, $\alpha = 0°$, $n = 0.6$, and Ra=10^4. In this figure, $x_1{}^*$ indicates the dimensionless length defined as: $x_1{}^* = \frac{x - R_i}{R_o - R_i}$. As shown, a negligible difference exists between 4941 and 8181 grids. Therefore, the mesh with 4941 grids was chosen for the following investigations.

3.2 The numerical method validation

Validation tests have been performed to make sure of the present simulation accuracy. First, the results of our numerical study were validated by those of an experimental study [39] and

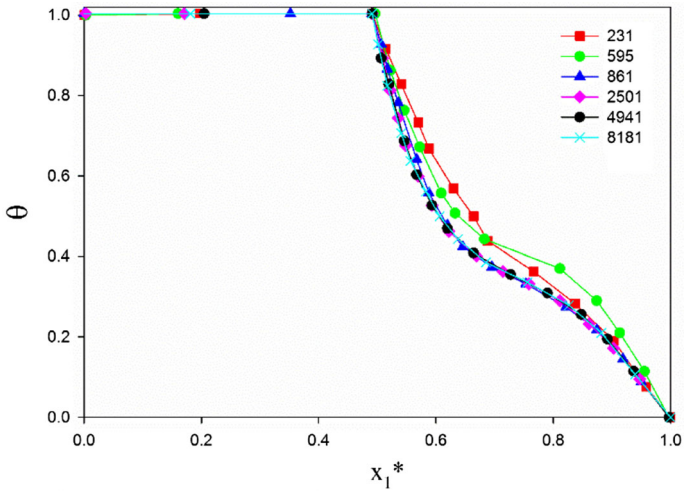

Fig. 2 Changes of θ, along $x_1{}^*$ inside the annulus for various mesh numbers, at Ra $= 10^4$, $\varphi = 90^\circ$, Pr $=$ 100, and $n = 0.6$

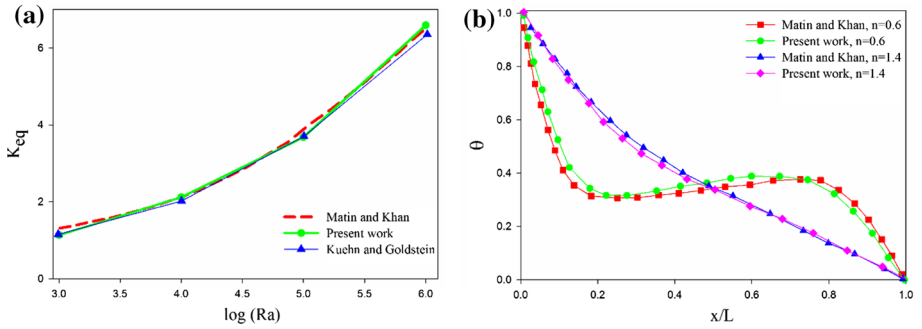

Fig. 3 **a** The results of the present study are compared with those of Kuehn and Goldstein [39], and Matin and Khan [35] for Newtonian flow ($R_o/R_i = 2.6$ and Pr $= 0.7$). **b** Comparison of θ variations between our results and those of ref. [35] for Ra=10^4 for two kinds of non-Newtonian fluid with $n = 0.6$ and $n = 1.4$

a numerical simulation [35]. The geometry in these studies was an annulus with the radius ratio of $R_o/R_i = 2.6$. Besides, the fluid has been considered as Newtonian with Pr $= 0.706$. Figure 3a depicts the average equivalent thermal conductivity (k_{eq}) computed from different studies. It is observable that the numerical results are compatible with the experimental ones.

Besides, the computed dimensionless temperature from simulation of power-law fluids in our work is validated with that reported in ref. [35] (as shown in Fig. 3b). As can be seen, our results are compatible with those of ref. [35]. Besides, Fig. 4 shows further validation illustrating changes of Nusselt number corresponding to the Ag-water nanofluid flow within two isothermally heated parallel plates under the effect of a magnetic field with the intensity of B_0. As can be seen, the present results match with the results of Karimipour et al. [16] by R-square [40, 41] of 98%.

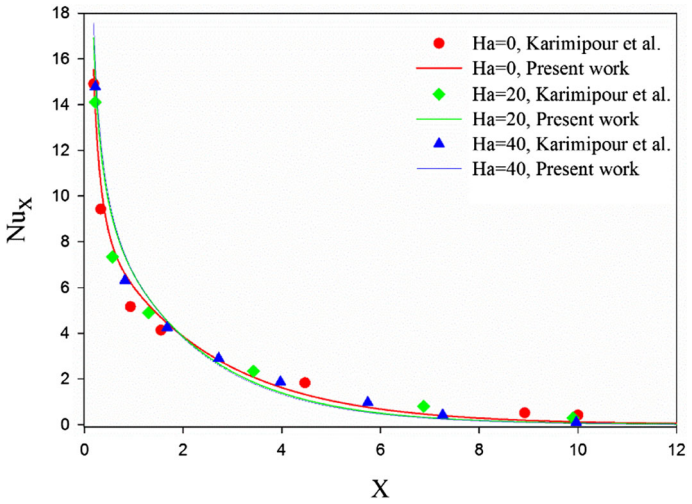

Fig. 4 Variation of Nu_x associated with the water-Ag nanofluid flowing within a microchannel at different values of Ha for $\omega = 0.04$, Re $= 10$, and B $= 0.05$

4 Result and discussion

4.1 Impacts of Rayleigh number and Hartmann number on heat transfer and fluid flow

Figure 5 illustrates isotherms and streamlines for nanofluid ($\omega = 0.02$) for various Hartmann numbers at $Ra = 10^4$, $n = 0.6$, Pr $= 100$, $R_o/R_i = 2.5$,α=0° and $L_f = 0.5$ where $L_f = \frac{l_f}{R_o - R_i}$.

When there is no magnetic field, two large loops due to buoyancy forces can be observed in streamline lines. By applying the magnetic field, the two loops break into smaller vortices due to the introduction of a magnetic volumetric force along a horizontal direction orthogonal to the buoyancy force (according to Eqs. 2 and 3). As the Hartmann number increases, the symmetry between the upper and lower regions of the cylinder increases. Among the studied Hartmann numbers, the streamlines at Ha $= 50$ show the maximum symmetry. This means that the fluid movement from the bottom to the top of the cylinder is diminished because the strong vortices that circulate the fluid at these two regions of the cylinder are weakened remarkably and have turned into smaller vortices which can be seen at the cylinder sides.

Besides, increasing the Hartmann number reduces the density of the nanofluid isotherms on the hot cylinder. Besides, the thickness of the boundary layer on the fins and the inner surface of the cylinder increases. It clarifies that augmentation of the Hartmann number declines the convection process generally. These observations are further confirmed by Fig. 6, illustrating the variation of K_{eq} as a function of *Ra* number at various values of Hartmann number. It can be observed that by increasing the *Ra* number, K_{eq} enhances the absence and presence of the magnetic field. While a reduction in the average equivalent thermal conductivity (K_{eq}) is observable by rising the Hartmann number at Ra numbers of 10^4 and 10^5. The magnetic force opposes the force of gravity and leads to a reduction of the net convective heat transfer. Besides, it is revealed that the impact of Hartmann number variations diminishes for smaller *Ra* numbers, such that for $Ra = 10^2$, Hartmann number exhibits almost no influence on the net convective heat transfer.

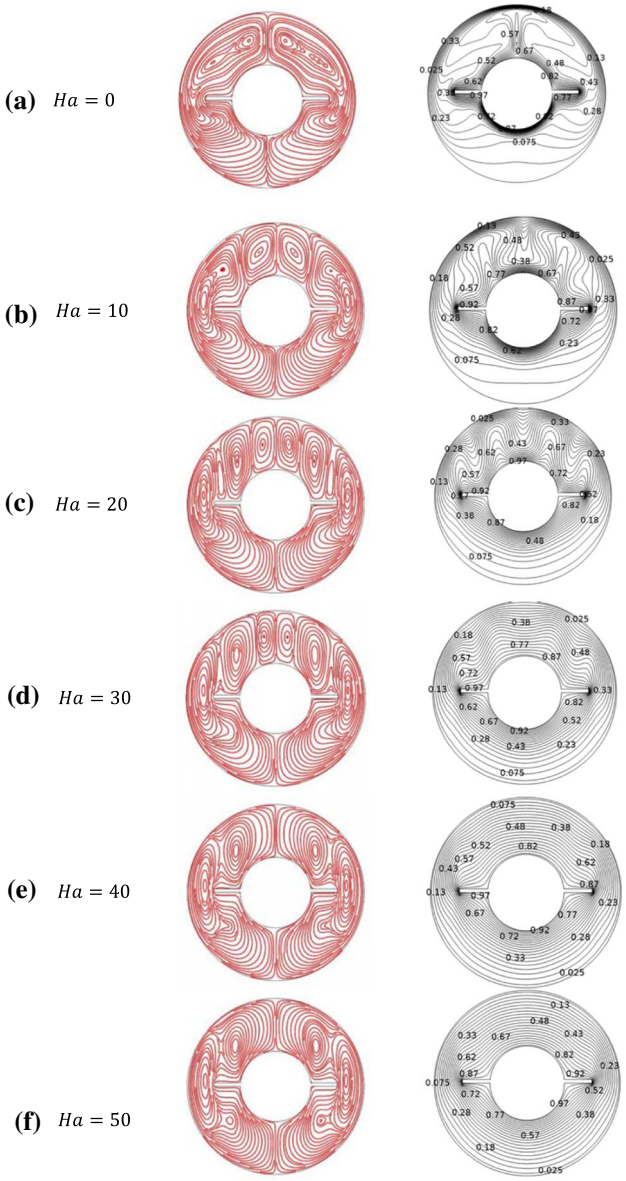

Fig. 5 The streamlines and isothermal lines are illustrated on the left and right sides of the figure, respectively, for different Hartmann numbers ($L_f = 0.5$, $n = 0.6$, $R_o/R_i = 2.5$, $Ra = 10^4$, α=0°, Pr = 100 and $\omega = 0.02$)

Figure 7a displays changes in the temperature profile with the Hartmann number across the annulus. According to this figure, it is obvious that as the Hartmann number rises, the curved shape of the temperature profiles alters to linear ones across the annulus, which demonstrates that conduction becomes the dominant form of heat transfer. Figure 7b provides comparisons of the vertical velocity profiles for various Hartmann numbers. It emerges that the vertical velocity falls as the Hartmann number rises. As can be observed, when the Hartmann number

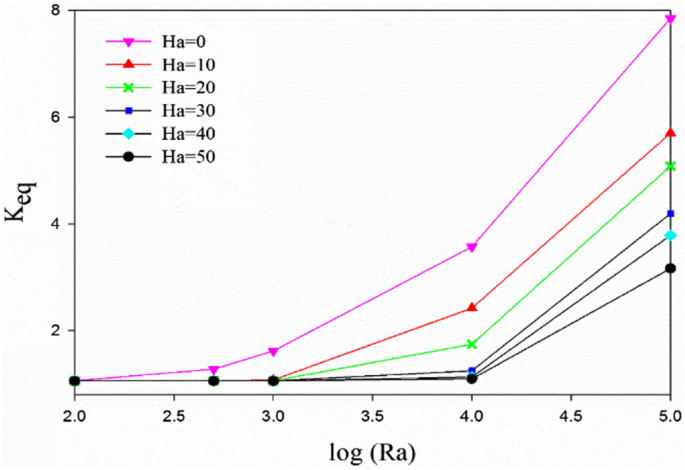

Fig. 6 Impact of Hartmann number on K_{eq} ($L_f = 0.5$, $n = 0.6$, Pr = 100, $R_o/R_i = 2.5$, α=0° and $\omega = 0.02$)

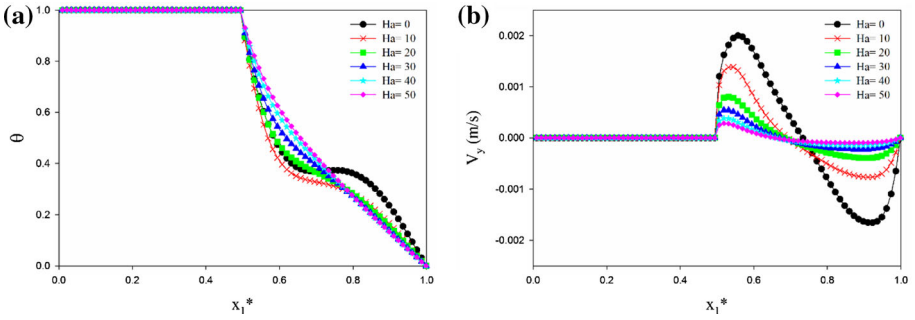

Fig. 7 **a** Dimensionless temperature distribution across the annulus for different Hartmann numbers ($L_f = 0.5$, Pr = 100, $R_o/R_i = 2.5$, $n = 0.6$, $\omega = 0.02$ and $Ra = 10^4$). **b** Variations of the vertical velocity across the annulus for different Hartmann numbers ($R_o/R_i = 2.5$, $Ra = 10^4$, $L_f = 0.5$, Pr = 100, and $n = 0.6$)

has a small value, the velocity variations across the annulus are sinusoidal. However, by augmentation of Hartmann number, the sinusoidal variations of velocity vanish gradually, and an approximately linear form is reached at values greater than Ha = 30, indicating that the conduction mechanism dominates the fluid flow

4.2 Effects of fins length on fluid flow and heat transfer

Figure 8 illustrates the effects of the fin length on the rate of free convection in the annulus with Ha = 20. For the case without any fin, six circulation loops can be observed. By adding horizontal fins to the inner cylinder surface, lateral vortices find more symmetry in the upper and lower parts. As far as the length of the fins increases, smaller vortices appear in the upper part of the cylinder. As the fin's length increases, fluid movement from the bottom to the upper region of the cylinder decreases. This is because more resistance against fluid circulation due to the buoyancy force is induced. Furthermore, it is observed that as the fins get longer, the density of the fluid isotherms on the hot cylinder decreases. It indicates that the elongation of fins suppresses the convection process between two cylinders. Figure 9 exhibits

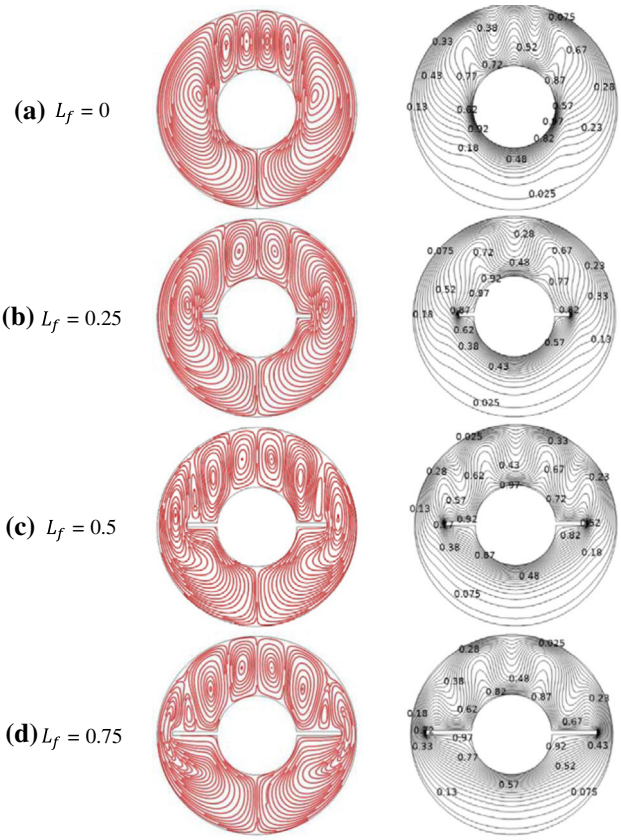

Fig. 8 The streamlines and isothermal lines are illustrated on the left and right sides of the figure, respectively, for different fin lengths ($n = 0.6$, $R_o/R_i = 2.5$, $Ra = 10^4$, Ha = 20, $\omega = 0.02$, Pr = 100 and α=0°)

these observations more quantitatively. According to this figure, the total heat transfer inside the annulus diminishes by increasing the fin length ratio L_f, which also was reported in our previous work [36].

4.3 Effects of the power-law index of non-Newtonian fluid on the heat transfer and flow characteristics

In Fig. 10, the variations of streamlines and isotherms are investigated for the annulus at various non-Newtonian power-law indices (n). When *n* increases, the number and the intensity of the vortices generated in the upper portion of the annulus decrease, and the isotherm lines in the annulus become more uniform. Besides, increasing the power-law index leads to the rise of viscosity of the fluid as well, and a stronger shear force is needed to keep the fluid in motion. Isotherm's density diminishes adjacent to the cylinders' wall leading to an increase in the thermal boundary layer thickness in these zones, which leads to the decrease in the convection heat transfer. It can be observed from Fig. 11 that increase in the power-law index results in the reduction of K_{eq}. However, it illustrates that for large values of the *Ha* number, the impact of *n* on the heat transfer inside the enclosure drops. At Hartmann number of Ha

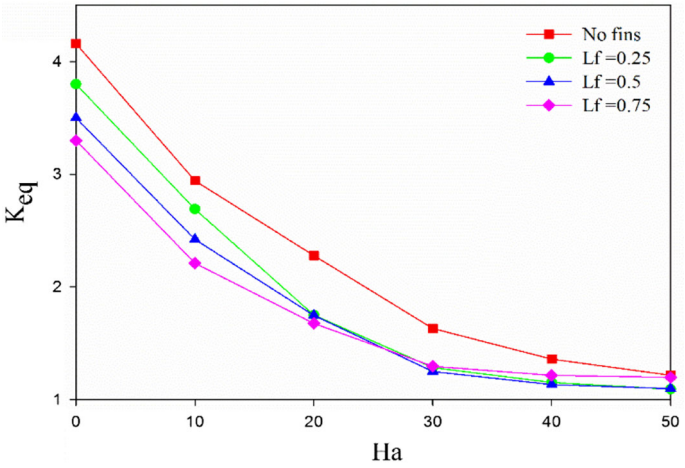

Fig. 9 Effects of fins length on total natural convection for different Hartmann numbers (Pr = 100, R_o/R_i = 2.5, n = 0.6, ω = 0.02 and Ra = 10^4)

= 50, K_{eq} corresponding to different values of n does not change significantly. Besides, for every power-law fluid, rising the Hartmann number results in a decrease in the net convective heat transfer. However, it is evident that when n increases, the influence of the Hartmann number diminishes, i.e., variations of the Hartmann number have a stronger influence on K_{eq} for power-law fluids with $n<1$ in comparison with the fluids with $n>1$. In fact, when we have $n<1$, fluid deformation can be carried out with less intensified shear stress, and these non-Newtonian fluids change more under the environmental changes.

As the *Ha* number rises, the symmetry between the upper and lower regions of the cylinder increases. Among the studied Hartmann numbers, the streamlines at Ha = 50 show the maximum symmetry. This means that the fluid movement from the bottom to the top of the cylinder is diminished because the strong vortices that circulate the fluid at these two regions of the cylinder are weakened remarkably and have turned into smaller vortices which is observable at the cylinder sides. Increasing the Hartmann number reduces the isotherms density on the hot cylinder. Besides, the boundary layer's thickness of the fins and the inner cylinder increases. It clarifies that augmentation of the Hartmann number declines the convection process generally.

Dimensionless temperature profiles are depicted in Fig. 12 (a) for $n = 0.6$ to 1.4. As shown, variations of the value of the power-law index alter the temperature profile substantially. As we move from $n = 0.6$ to $n = 1.4$, the temperature profile between two cylinders moves toward a straight line indicating the dominance of conduction heat transfer for larger power-law indices. This is because of increasing the shear stress at the fluid layers, which leads to weaker convection heat transfer within the annulus. Figure 12 (b) illustrates variations of the vertical velocity with the power-law index "n". As can be seen, magnitudes of vertical velocity become smaller within the annulus for larger power-law indices. The velocity magnitude of the shear-thickening non-Newtonian fluid with $n = 1.4$ is near to zero.

4.4 Variations of solid nanoparticles volume fraction

Figure 13 depicts variations of K_{eq} as a function of Ra number at various volume fractions. Augmentation of the volume fraction results in thermal conductivity improvement, which

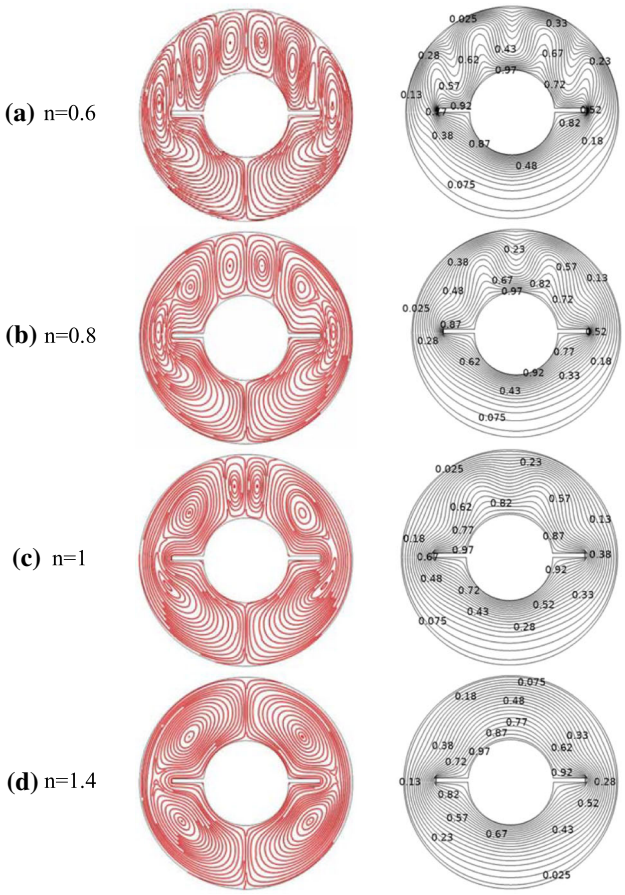

Fig. 10 The streamlines and isothermal lines are illustrated on the left and right sides of the figure, respectively, for different values of n (Pr = 100, $R_o/R_i = 2.5$, Ha = 20, $\omega = 0.02$, $L_f = 0.5$, and Ra = 10^4)

leads to heat transfer enhancement and K_{eq} as well. As can be seen, there is a better enhancement in total heat in low Rayleigh numbers due to the addition of the nanoparticles. Because in this range of Ra, conduction is the dominant form of heat transfer. For instance, the increase in the average equivalent thermal conductivity due to nanoparticle addition with $\omega = 0.05$ is substantially larger (~ 70%) for Ra = 10^2 and Ha = 20 in comparison with the case of Ra = 10^5 (~ 15%).

Average equivalent thermal conductivity (K_{eq}) is plotted in Fig. 14 as a function of Hartmann number for various volume fractions. As mentioned in previous sections, K_{eq} increases gradually as a result of volume fraction augmentation, and it decreases with Hartmann number. Also, this figure shows a remarkable reduction in the difference between average equivalent thermal conductivity values of various volume fractions as the Hartmann number rises.

4.5 Variations of fins inclination angle and Prandtl number

Figure 15a represents the variations of K_{eq} relative to the fins inclination angle (α) at different Hartmann numbers for the non-Newtonian fluids with an index less than one (shear-thinning

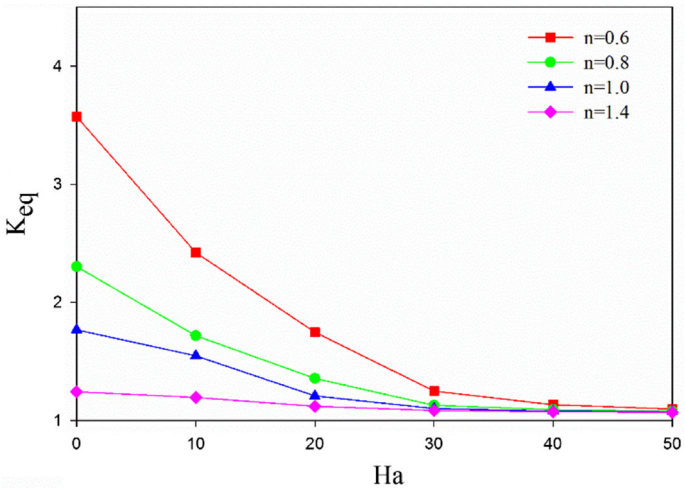

Fig. 11 Effects of n on K_{eq} for different Hartmann numbers ($L_f = 0.5$, Pr $= 100$, $R_o/R_i = 2.5$, $\omega = 0.02$, and Ra $= 10^4$)

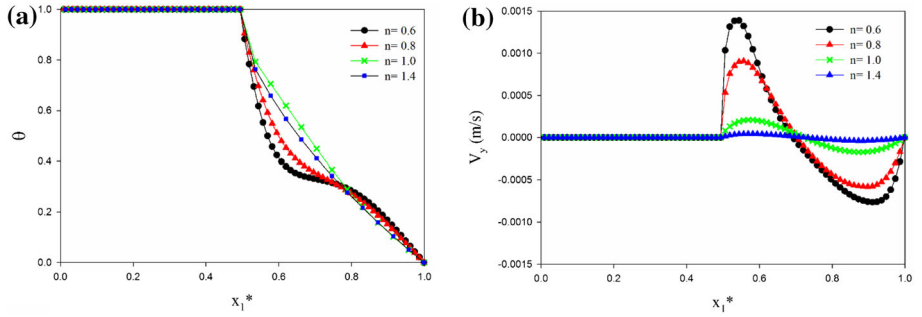

Fig. 12 **a** Dimensionless temperature distribution across the annulus. **b** Vertical velocity within the annulus for various values of n ($L_f = 0.5$, Pr $= 100$, $R_o/R_i = 2.5$, $\omega = 0.02$, and Ra $= 10^4$)

fluids). As can be observed in this figure, when no magnetic field is applied (Ha $= 0$), a marginal increase in K_{eq} occurs for augmentation of fins inclination angle larger than about $\alpha = 50^{\circ}$. However, for a larger *Ha* number, as the magnetic force dominates, the fin angle effect on K_{eq} becomes negligible. Figure 15b shows the changes in the average equivalent thermal conductivity (K_{eq}) against Pr number at different *Ha* numbers. At lower values of Hartmann number, by increasing the Pr number, natural convection inside the cylinders gets better, and K_{eq} increases as well. However, by augmentation of Hartmann number, the magnetic body force overcomes the buoyancy force, and the impact of Pr on K_{eq} becomes almost negligible

5 Conclusion

In the present study, heat transfer of natural convection inside an annulus with two internal fins, containing non-Newtonian nanofluid, under the influence of vertical magnetic field is

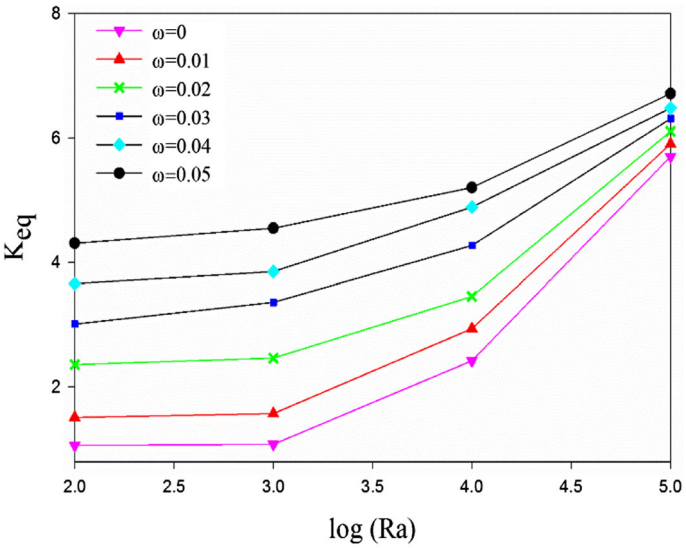

Fig. 13 Effects of volume fraction on K_{eq} ($L_f = 0.5$, $n = 0.6$, Pr = 100, $R_o/R_i = 2.5$, α=0°, $\omega = 0.02$, and Ha = 20)

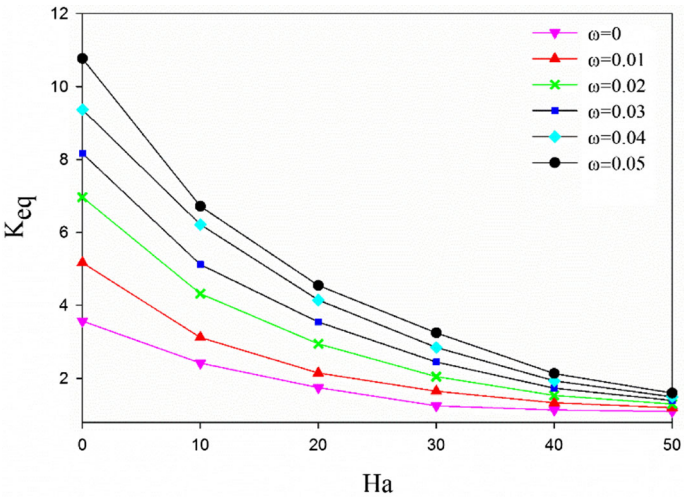

Fig. 14 Effects of the volume fraction on K_{eq} for different Hartmann numbers ($L_f = 0.5$, Pr = 100, $R_o/R_i = 2.5$, $\omega = 0.02$, and $Ra = 10^4$)

investigated. This study has been carried out for various parameters of Hartmann number, Rayleigh number, volume fraction, power-law index, Prandtl number, fin length ratio, and fin inclination angle. The most important findings of this study are given in the following sentences:

- As the Hartmann number rises, the magnetic force opposes the force of gravity and declines the convection process generally.

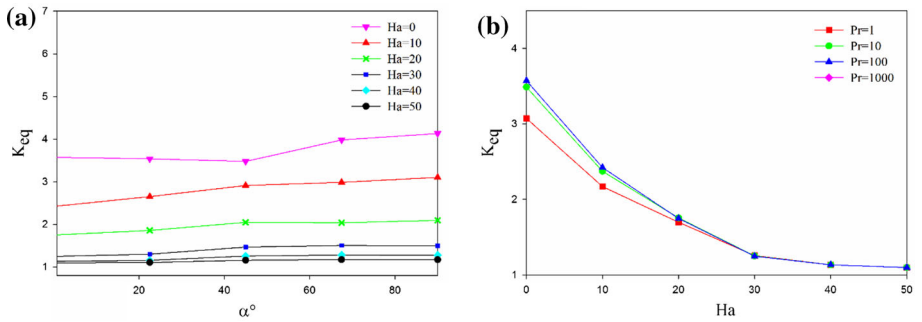

Fig. 15 Variations of K_{eq} with **a** the fins angles for various Hartmann numbers **b** Pr number at ($L_f = 0.5$, $R_o/R_i = 2.5$, $\omega = 0.02$, and $Ra = 10^4$)

- Increasing the Rayleigh number leads to the net convective heat transfer improvement in various Hartmann numbers. The effect of Hartmann number alteration on the average equivalent thermal conductivity (K_{eq}) weakens for smaller *Ra* numbers, such that for *Ra* $= 10^2$, Hartmann number alteration has almost no influence on the net convective heat transfer.
- When the fins length increases, the fluid isotherms density on the hot cylinder diminishes, and consequently, the heat transfer between two cylinders drops remarkably.
- For shear-thinning fluids with a power-law index less than 1, the Ha number imposes a stronger effect on the heat transfer process than the shear-thickening fluids.
- Augmentation of the solid nanoparticles results in thermal conductivity enhancement and, consequently, heat transfer improvement. This effect was more intensified in low Rayleigh. Also, a reduction in the difference between K_{eq} values for various volume fractions has been observed as the Hartmann number rises.
- When no magnetic field is implemented in the annulus ($Ha = 0$), a marginal increase in K_{eq} occurs with augmentation of fins inclination angle. However, for large *Ha* numbers, the fin angle effect on K_{eq} becomes negligible.

Declarations

Conflict of Interest The authors declare that they have no conflict of interest.

References

1. A. Dogonchi, M.A. Ismael, A.J. Chamkha, D. Ganji, Numerical analysis of natural convection of Cu–water nanofluid filling triangular cavity with semicircular bottom wall. J. Therm. Anal. Calorim. **135**(6), 3485–3497 (2019)
2. A.J. Chamkha, A. Dogonchi, D. Ganji, Magneto-hydrodynamic flow and heat transfer of a hybrid nanofluid in a rotating system among two surfaces in the presence of thermal radiation and Joule heating. AIP Adv. **9**(2), 025103 (2019)
3. A.I. Alsabery, M.A. Ismael, A.J. Chamkha, I. Hashim, H. Abulkhair, Unsteady flow and entropy analysis of nanofluids inside cubic porous container holding inserted body and wavy bottom wall. Int. J. Mech. Sci. **193**, 106161 (2021)

4. T. Tayebi and A. J. Chamkha, Magnetohydrodynamic natural convection heat transfer of hybrid nanofluid in a square enclosure in the presence of a wavy circular conductive cylinder. J. Therm. Sci. Eng. Appl. **12**(3), 031009 (2020)
5. Q.-H. Deng, J.-J. Chang, Natural convection in a rectangular enclosure with sinusoidal temperature distributions on both side walls. Numer. Heat Transf. Part A Appl. **54**(5), 507–524 (2008). https://doi.org/10.1080/01457630802186080
6. S. Inoue, Y. Iba, Y. Matsumura, Drastic enhancement of effective thermal conductivity of a metal hydride packed bed by direct synthesis of single-walled carbon nanotubes. Int. J. Hydrogen Energy **37**(2), 1836–1841 (2012). https://doi.org/10.1016/j.ijhydene.2011.10.031
7. C.J. Ho, W.K. Liu, Y.S. Chang, C.C. Lin, Natural convection heat transfer of alumina-water nanofluid in vertical square enclosures: an experimental study. Int. J. Therm. Sci. **49**(8), 1345–1353 (2010). https://doi.org/10.1016/j.ijthermalsci.2010.02.013
8. S. Soleimani, M. Sheikholeslami, D.D. Ganji, M. Gorji-Bandpay, Natural convection heat transfer in a nanofluid filled semi-annulus enclosure. Int. Commun. Heat Mass Transfer **39**(4), 565–574 (2012). https://doi.org/10.1016/j.icheatmasstransfer.2012.01.016
9. M. Sheikholeslami, M. Gorji-Bandpy, D.D. Ganji, Lattice Boltzmann method for MHD natural convection heat transfer using nanofluid. Powder Technol. **254**, 82–93 (2014). https://doi.org/10.1016/j.powtec.2013.12.054
10. F. Selimefendigil, H.F. Öztop, Natural convection and entropy generation of nanofluid filled cavity having different shaped obstacles under the influence of magnetic field and internal heat generation. J. Taiwan Inst. Chem. Eng. **56**, 42–56 (2015). https://doi.org/10.1016/j.jtice.2015.04.018
11. A. Malekpour, N. Karimi, A. Mehdizadeh, "Magnetohydrodynamics, natural convection and entropy generation of CuO-water nanofluid in an I-shape enclosure. J. Therm. Sci. Eng. Appl. **10**, 061016 (2018)
12. G.R. Kefayati, Simulation of heat transfer and entropy generation of MHD natural convection of non-Newtonian nanofluid in an enclosure. Int. J. Heat Mass Transfer **92**, 1066–1089 (2016). https://doi.org/10.1016/j.ijheatmasstransfer.2015.09.078
13. F. Selimefendigil, A. J. Chamkha, MHD mixed convection of nanofluid in a three-dimensional vented cavity with surface corrugation and inner rotating cylinder, Int. J. Numer. Methods Heat Fluid Flow, 2019.
14. A.I. Alsabery, T. Armaghani, A.J. Chamkha, I. Hashim, Two-phase nanofluid model and magnetic field effects on mixed convection in a lid-driven cavity containing heated triangular wall. Alex. Eng. J. **59**(1), 129–148 (2020)
15. T. Tayebi, A. J. Chamkha, Entropy generation analysis during MHD natural convection flow of hybrid nanofluid in a square cavity containing a corrugated conducting block, Int. J. Numer. Methods Heat Fluid Flow, 2019
16. A. Karimipour, A. D'Orazio, M.S. Shadloo, The effects of different nano particles of Al2O3 and Ag on the MHD nano fluid flow and heat transfer in a microchannel including slip velocity and temperature jump. Physica E **86**, 146–153 (2017). https://doi.org/10.1016/j.physe.2016.10.015
17. R. Alizadeh, N. Karimi, R. Arjmandzadeh, A. Mehdizadeh, Mixed convection and thermodynamic irreversibilities in MHD nanofluid stagnation-point flows over a cylinder embedded in porous media. J. Therm. Anal. Calorim. **135**(1), 489–506 (2019)
18. F. Selimefendigil, H.F. Öztop, Conjugate natural convection in a cavity with a conductive partition and filled with different nanofluids on different sides of the partition. J. Mol. Liquids **216**, 67–77 (2016). https://doi.org/10.1016/j.molliq.2015.12.102
19. M.S. Kandelousi, Effect of spatially variable magnetic field on ferrofluid flow and heat transfer considering constant heat flux boundary condition. Eur Phys. J. Plus **129**(11), 248 (2014). https://doi.org/10.1140/epjp/i2014-14248-2
20. A. Malvandi, M.H. Kaffash, D.D. Ganji, Nanoparticles migration effects on magnetohydrodynamic (MHD) laminar mixed convection of alumina/water nanofluid inside microchannels. J. Taiwan Inst. Chem. Eng. **52**, 40–56 (2015). https://doi.org/10.1016/j.jtice.2015.02.008
21. T. Hayat, Z. Nisar, H. Yasmin, A. Alsaedi, Peristaltic transport of nanofluid in a compliant wall channel with convective conditions and thermal radiation. J. Mol. Liquids **220**, 448–453 (2016). https://doi.org/10.1016/j.molliq.2016.04.080
22. A. Malvandi, Film boiling of magnetic nanofluids (MNFs) over a vertical plate in presence of a uniform variable-directional magnetic field. J. Magn. Magn. Mater. **406**, 95–102 (2016). https://doi.org/10.1016/j.jmmm.2016.01.008
23. A. Saeed, N. Karimi, G. Hunt, M. Torabi, On the influences of surface heat release and thermal radiation upon transport in catalytic porous microreactors—a novel porous-solid interface model. Chem. Eng. Process. Process Intensif. **143**, 107602 (2019)

24. M.A. Sheremet, H.F. Oztop, I. Pop, MHD natural convection in an inclined wavy cavity with corner heater filled with a nanofluid. J. Magn. Magn. Mater. **416**, 37–47 (2016). https://doi.org/10.1016/j.jmmm.2016.04.061
25. M. Sheikholeslami, D.D. Ganji, Influence of magnetic field on CuO–H2O nanofluid flow considering Marangoni boundary layer. Int. J. Hydrogen Energy **42**(5), 2748–2755 (2017). https://doi.org/10.1016/j.ijhydene.2016.09.121
26. M. Sheikholeslami, Magnetic field influence on CuO–H2O nanofluid convective flow in a permeable cavity considering various shapes for nanoparticles. Int. J. Hydrogen Energy **42**(31), 19611–19621 (2017). https://doi.org/10.1016/j.ijhydene.2017.06.121
27. M. Sheikholeslami, M. Shamlooei, Fe3O4–H2O nanofluid natural convection in presence of thermal radiation. Int. J. Hydrogen Energy **42**(9), 5708–5718 (2017). https://doi.org/10.1016/j.ijhydene.2017.02.031
28. M. Miao, Electrical conductivity of pure carbon nanotube yarns. Carbon **49**(12), 3755–3761 (2011). https://doi.org/10.1016/j.carbon.2011.05.008
29. Z. Han, A. Fina, Thermal conductivity of carbon nanotubes and their polymer nanocomposites: a review. Progress Polym. Sci. **36**(7), 914–944 (2011). https://doi.org/10.1016/j.progpolymsci.2010.11.004
30. N.R. Pradhan, H. Duan, J. Liang, G.S. Iannacchione, The specific heat and effective thermal conductivity of composites containing single-wall and multi-wall carbon nanotubes. Nanotechnology **20**(24), 245705 (2009). https://doi.org/10.1088/0957-4484/20/24/245705
31. M. Ghasemian, Z.N. Ashrafi, M. Goharkhah, M. Ashjaee, Heat transfer characteristics of Fe3O4 ferrofluid flowing in a mini channel under constant and alternating magnetic fields. J. Magn. Magn. Mater. **381**, 158–167 (2015)
32. F. Selimefendigil, H.F. Öztop, Conjugate natural convection in a nanofluid filled partitioned horizontal annulus formed by two isothermal cylinder surfaces under magnetic field. Int. J. Heat Mass Transf. **108**, 156–171 (2017)
33. M.R.D. Garmroodi, A. Ahmadpour, M.R. Hajmohammadi, S. Gholamrezaie, Natural convection of a non-Newtonian ferrofluid in a porous elliptical enclosure in the presence of a non-uniform magnetic field. J. Therm. Anal. Calorim. **141**(5), 2127–2143 (2020)
34. D.S. Udawattha, M. Narayana, U.P.L. Wijayarathne, Predicting the effective viscosity of nanofluids based on the rheology of suspensions of solid particles. J. King Saud Univ. Sci. (2017). https://doi.org/10.1016/j.jksus.2017.09.016
35. M.H. Matin, W.A. Khan, Laminar natural convection of non-Newtonian power-law fluids between concentric circular cylinders. Int. Commun. Heat Mass Transfer **43**, 112–121 (2013)
36. H. Hadidi, M.K.D. Manshadi, R. Kamali, Natural convection of power-law fluids inside an internally finned horizontal annulus. Iran. J. Sci. Technol. Trans. Mech. Eng. (2018). https://doi.org/10.1007/s40997-018-0269-3
37. M. Amoura, N. Zeraibi, A. Smati, M. Gareche, Finite element study of mixed convection for non-Newtonian fluid between two coaxial rotating cylinders. Int. Commun. Heat Mass Transfer **33**(6), 780–789 (2006). https://doi.org/10.1016/j.icheatmasstransfer.2006.02.020
38. N. D. Francis, Jr., M. T. Itamura, S. W. Webb, and D. L. James, "CFD Calculation of Internal Natural Convection in the Annulus between Horizontal Concentric Cylinders," United States, 2002. [Online]. Available: http://inis.iaea.org/search/search.aspx?orig_q=RN:35089215
39. T. Kuehn, R. Goldstein, An experimental and theoretical study of natural convection in the annulus between horizontal concentric cylinders. J. Fluid Mech. **74**(4), 695–719 (1976)
40. S.M. Mousavi, E. Roohi, Large eddy simulation of shock train in a convergent–divergent nozzle. Int. J. Mod. Phys. C **25**(04), 1450003 (2014)
41. A. Binesh, S. Mousavi, R. Kamali, Effect of temperature-dependency of Newtonian and non-Newtonian fluid properties on the dynamics of droplet impinging on hot surfaces. Int. J. Mod. Phys. C **26**(09), 1550106 (2015)